Structures 80 (2025) 110035

Contents lists available at ScienceDirect

Structures

journal homepage: www.elsevier.com/locate/structures

# Polynomial chaos expansion-driven Bayesian inference for multi-parameter identification of large-span curved footbridge

Zhifan Han [a], Yifei Li [b,*], Magd Abdel Wahab [c,d]

[a] School of Architectural Engineering, Guangzhou Institute of Science and Technology, Guangzhou 510540, China
[b] School of Engineering, Huzhou University, Huzhou 313000, China
[c] Soete Laboratory, Department of Electrical Energy, Metals, Mechanical Constructions, and Systems, Faculty of Engineering and Architecture, Ghent University, Gent, Belgium
[d] Parallel and Distributed Systems Laboratory, Jožef Stefan Institute, Jamova cesta 39, Ljubljana SI-1000, Slovenia

ARTICLE INFO

*Keywords:*
Footbridge
Polynomial chaos expansion
Bayesian inference
Parameters identification
Probabilistic Finite Element Analysis

ABSTRACT

Parameter identification plays a crucial role in the design, construction, and operation of large-span footbridges. This paper proposes a novel PCE-BI method combining Polynomial Chaos Expansion (PCE) and Bayesian Inference (BI) for multi-parameter identification of footbridges. First, a lightweight and reliable PCE surrogate model is established based on Latin hypercube sampling and probabilistic Finite Element Analysis (FEA), replacing the Finite Element (FE) model of the footbridge. Subsequently, PCE-driven Bayesian inference is used to identify unknown parameters, directly avoiding the high computational cost of FEA. Additionally, the Borgonovo sensitivity analysis method is integrated with PCE to achieve near-zero-cost sensitivity analysis of footbridge parameters. The effectiveness and practicality of the PCE-BI method are verified through a case study of a large-span curved footbridge. Compared with traditional iteration-based parameter identification methods, the PCE-BI method achieves a 31.8-fold reduction in computational time while simultaneously enhancing identification accuracy. The proposed method is suitable for multi-parameter identification of complex large-span bridges and can be extended to other large-scale structures.

## 1. Introduction

Large-span footbridges serve as vital transportation infrastructure and play an irreplaceable role in urban development [1,2]. However, during long-term service, material aging, fatigue, crack propagation, and other factors can degrade their mechanical properties, potentially leading to excessive vibration and hidden safety hazards [3,4]. Therefore, conducting structural safety assessment for large-span footbridges is crucial to ensuring their long-term safe and reliable operation.

Structural safety assessment typically relies on accurate input parameters for structural models, including material properties, boundary conditions, etc., which are often difficult to obtain directly or may change over service time. Therefore, structural parameter identification techniques are required to infer model parameters from measured data. The updated model obtained through parameter identification can more realistically reflect the current state of the structure, providing a reliable foundation for structural safety assessment and playing an irreplaceable role in structural health monitoring [5].

Traditional parameter identification methods typically rely on deterministic optimization frameworks and employ early optimization algorithms such as gradient descent. These methods quantify the discrepancy between Finite Element (FE) model predictions and measured response data by constructing an objective function, then iteratively adjust parameters to minimize this discrepancy, thereby estimating structural parameters [6]. However, traditional methods fail to fully account for the inherent randomness of material parameters and depend on searching for a single optimal solution, leading to low computational efficiency. They are generally suitable only for simple structures under uniform working conditions, falling short of the high-precision and high-efficiency requirements of modern engineering [7,8].

To overcome the limitations of traditional methods, machine learning methods have been introduced into the field of parameter identification, addressing parameter inversion problems in complex scenarios through data-driven approaches [9,10]. In the field of mechanical engineering, for both structural parameter identification and

* Corresponding author.
*E-mail address:* 03354@zjhu.edu.cn (Y. Li).

https://doi.org/10.1016/j.istruc.2025.110035
Received 26 June 2025; Received in revised form 20 August 2025; Accepted 21 August 2025
Available online 28 August 2025

load parameter identification, Artificial Neural Network (ANN), Convolutional Neural Network (CNN), and collaborative clustering algorithms have been effectively applied, providing feasible solutions to related problems in this domain [11–13]. However, traditional data-driven methods suffer from insufficient interpretability, along with challenges such as poor out-of-distribution prediction performance and inadequate model stability, which restrict their application in civil engineering structural parameter identification. In recent years, frameworks based on Physics-Informed Neural Network (PINN) have been able to alleviate the aforementioned drawbacks of machine learning methods by embedding physical constraints into the loss function during training [14]. Nevertheless, this method incurs high computational costs due to the need to handle high-order derivatives and multi-physics coupling, and it is currently mainly applied to simple structures such as beams and plates. It is thus evident that a single algorithm struggles to balance accuracy and efficiency in parameter identification for large and complex structures [15–17].

In recent years, for parameter identification in complex engineering structures, surrogate models have been widely adopted to avoid repeated calls to FE models while incorporating uncertainties in material parameters [18,19]. Surrogate models efficiently characterize the mapping relationship between random input parameters and system responses or Quantities of Interest (QoIs), significantly reducing computational costs while maintaining high-precision outputs. Common surrogate models include Kriging, Support Vector Regression (SVR), and Polynomial Chaos Expansion (PCE) [20–23].

### 1.1. Application of PCE for bridges

PCE maps the randomness of input parameters into a linear combination of orthogonal polynomial bases. Through Latin Hypercube Sampling (LHS) and sparse truncation strategies, such as hyperbolic truncation, high-precision models can be constructed with only a small number of samples [24–26]. Wu et al. [27] applied PCE models to formulate bridge-vehicle system equations, combining spectral stochastic FEA to analyze uncertainties in bridge-vehicle interaction problems. Spiridonakos et al. [28] used PCE models to establish relationships between bridge structural responses and external influencing factors, which is used for predicting structural responses, extracting structural performance indicators, and integrating environmental uncertainties into structural analysis. Ni et al. [29] conducted uncertainty quantification and global sensitivity analysis using PCE models, demonstrating that PCE models perform well in eigenvalue analysis of simply supported bridges and response analysis of bridge-vehicle systems. Rizzo et al. [30] leveraged PCE models to generate uncertain flutter derivative datasets, expanding experimental data to support calculations of critical flutter speeds for suspension bridges. Wan et al. [31] proposed a arbitrary PCE model for uncertainty quantification and global sensitivity analysis in structural dynamics, which is applied to a long-span steel arch bridge. Shang et al. [32] developed an extremum-oriented sensitivity analysis method combining PCE to evaluate sensitivities of structural extreme responses and limit states, and validated and applied it in dynamic train-track-bridge systems. Hu et al. [33] used both PCE and Kriging surrogate models to study uncertainties in buffeting analysis of long-span bridges, approximating structural responses with surrogates and reducing input variables via parameter sensitivity analysis. Wei et al. [34] performed uncertainty quantification and global sensitivity analysis on full-scale all-FRP footbridges using PCE models, investigating how uncertainties in FRP material mechanical properties affect bridge dynamic responses.

### 1.2. Parameter identification of bridges using Bayesian inference

For parameter identification, Bayesian inference integrates prior knowledge and observation data through a probabilistic framework, treating parameters as random variables and describing parameter uncertainties via posterior distributions. This approach overcomes the limitations of traditional deterministic optimization methods, such as gradient descent, which struggle to quantify uncertainties and are prone to local optima [35,36]. Conde et al. [37] combined a Gaussian process emulator with Bayesian inference for parameter identification of a masonry arch bridge, using the emulator to replace the original FE model and reduce computational costs. Jesus et al. [38] proposed a modular Bayesian framework that accounts for temperature and traffic load effects to identify key parameters of the Tamar suspension bridge. Argyris et al. [39] developed a Bayesian inference framework for parameter identification of highway bridges and adjacent soils. They used Component Mode Synthesis (CMS) to reduce computational costs and employed the Transitional Markov Chain Monte Carlo (TMCMC) algorithm for model parameter estimation. Ni et al. [40] adopted a parameter identification method based on variational Bayesian inference, approximating complex likelihood functions via adaptive Gaussian process modeling and using Gaussian mixture models to describe unknown posterior probability distributions, thereby identifying unknown parameters of simply supported beams under moving loads. Liu et al. [41] proposed a Bayesian inference-based method to identify vortex-excited force parameters of long-span bridges using field-measured vibration data. Lima et al. [42] developed a variational Bayesian inference-based parameter identification method, constructing forward models via Proper Generalized Decomposition (PGD) to reduce computational costs for multi-dimensional problems, which was validated in multiple cases including a small reinforced bridge.

### 1.3. Contributions and objectives

In summary, PCE models and Bayesian inference have diverse applications in bridge engineering. PCE models are primarily used for sensitivity analysis and uncertainty handling in bridge engineering, with limited research applying them to identify unknown material parameters. Bayesian inference effectively addresses uncertainties such as material properties and measurement errors, which is suitable for complex models and is widely used in bridge parameter identification. However, its high computational cost limits its practical applications. PCE models, by contrast, can accurately construct surrogate models for footbridges at extremely low computational costs, effectively replacing computationally intensive FE models of footbridges. Therefore, based on the characteristics of human-induced vibrations in large-span footbridges, this study proposed a PCE-BI method which combines PCE and Bayesian inference for multi-parameter identification of footbridges. The main contributions are as follows:

- Develop a lightweight and reliable PCE surrogate model to replace the time-consuming FEA of footbridges, thereby significantly enhancing computational efficiency.
- Integrate the Borgonovo sensitivity analysis method with PCE to enable near-zero-cost sensitivity analysis of footbridge parameters.
- Employ the PCE-BI method for parameter identification of footbridges, which substantially reduces computational time while maintaining high accuracy, thus demonstrating strong engineering applicability.

Using a large-span curved footbridge as an engineering case, this study validates the applicability of the PCE-BI method under complex human-induced vibration environments. It provides an efficient solution for parameter identification in large-span flexible structures and offers a valuable reference for health monitoring, and vibration control of similar structures.

This article is organized as follows. Section 2 briefly reviews the fundamentals of PCE and BI. Section 3 presents the procedure and evaluation metrics of the PCE-BI method. Section 4 constructs a PCE model for the curved footbridge, comparing it with Kriging and SVR models. Section 5 describes the parameters identification of the curved footbridge using the PCE-BI method. Finally, Section 6 summarizes the conclusions of this study.

## 2. Theoretical fundamentals

### 2.1. Polynomial Chaos Expansion (PCE)

PCE is an effective tool for dealing with uncertainty problems. Its core lies in approximating the output of a computational model (e.g., FE model) using input random variables with the aid of orthogonal polynomials [43,44]. Suppose that there exists an M-dimensional random vector $X = x_1, x_2, \cdots, x_M$, described by the joint probability density functions$f_{x_j}$,where $j = 1, 2, M$. The output of the system $Y = \mathscr{M}(X)$ is also a random variable [45]. $Y$can be expanded infinitely through PCE as follows:

$$Y = \mathscr{M}(X) \approx \mathscr{M}^{PCE}(X) = \sum_{\theta \in \mathscr{A}} \xi_{\theta} \varphi_{\theta}(x) \tag{1}$$

where $\theta = \{\theta_1, \cdots, \theta_M\}(\theta_j \geq 0) \in \mathscr{A}$ is a multi-index symbolic vector used to determine the form of the multivariate polynomials; $\mathscr{A} \in \mathbb{N}^M$is a multi-index truncation set that limits the polynomial combinations involved in the calculation; $\xi_\theta \in \mathbb{R}$ is the expansion coefficients to be determined; $\varphi_\theta(X) = \prod_{j=1}^{M} \psi_{\theta_j}^{(j)}(x_j)$ is a multivariate polynomial orthogonal to $f_x$ and $\psi_{\theta_j}^{(j)}$ is a univariate orthogonal polynomial of degree $\theta_j$ for the $j$-th variable. This orthogonality facilitates subsequent calculations and analyses.

According to the "sparsity-of-effects principle", most models describing physical phenomena are dominated by main effects and low-order interactions. Therefore, in practical applications, Eq. (1) needs to be truncated appropriately. Common truncation schemes include standard truncation and hyperbolic truncation [46]. Standard truncation corresponds to all polynomials with a total degree less than or equal to $p$ for $M$ input variables, as follows:

$$\mathscr{A}^{M,p} = \theta \in \mathbb{N}^M : |\theta| \leq p \ \text{card}\mathscr{A}^{M,p} \equiv P = \binom{M+p}{p} = \frac{(M+p)!}{p!M!} \tag{2}$$

where $p$ is the polynomial degree, and $P$ is the total-degree basis, which grows exponentially with $p$.

As $p$ and $M$ increase, the computational amount grows rapidly. As an improvement of the standard truncation scheme, hyperbolic truncation defines the truncation range by introducing a truncation number $q$:

$$\mathscr{A}^{\mathscr{M},p,q} = \left\{\theta \in \mathscr{A}^{\mathscr{M},p} : \left\|\theta_q\right\| \leq p\right\}, \quad \|\theta\|_q = \left(\sum_{i=1}^{M} \theta_i^q\right)^{1/q} \tag{3}$$

When $q = 1$, hyperbolic truncation is equivalent to standard truncation, whereas when $q < 1$, the number of high-order interaction polynomials and the number of model evaluations can be reduced. Meanwhile, by using the "sparsity-of-effects principle", even when some high-order terms are removed, the model accuracy can be maintained or even improved. Fig. 1 shows the variations of $q$ and $p$ in hyperbolic truncation.

After the above truncation, Eq. (1) can be rewritten as follows:

$$Y = \mathscr{M}(X) = \sum_{j=0}^{P-1} \xi_j \phi_j(x) + \varepsilon_p \equiv \xi^T \phi(x) + \varepsilon_p \tag{4}$$

where $\varepsilon_p$ is the truncation error, $p$ is determined according to the selected truncation scheme, the superscript $T$ represents transposition, and $\xi = \{\xi_0, \cdots, \xi_{P-1}\}^T$ is a vector containing expansion coefficients.

Eq. (4) reflects the transition from the ideal infinite expansion to a practically computable form, clarifying the key variables, which is crucial for constructing a complete theoretical framework of the PCE model.

Among the numerous methods for calculating the coefficients of the PCE model, this study adopts the Orthogonal Matching Pursuit (OMP) algorithm. OMP is a greedy algorithm that constructs a sparse PCE model by iteratively selecting polynomial basis elements most relevant to the current residual. These selected basis elements are then added to the active set [47]. It can effectively screen out polynomial basis elements that have a significant impact on the model output, reduce unnecessary calculations, improve computational efficiency, and still maintain good performance in high-dimensional cases.

### 2.2. PCE-based Borgonovo indices for sensitivity analysis

The derivation of the Borgonovo indices is independent of the structure of input variables, and it is applicable whether the input variables are independent or correlated. This feature gives it significant advantages in handling complex practical engineering problems, enabling a wide range of application scenarios. The Borgonovo index $\delta_i$ provides a moment-independent global sensitivity measure by quantifying the expected shift in the output probability distribution when the input variable $x_i$ is fixed [48]. This index is defined as:

$$\delta_i = \frac{1}{2}\int_{D_{X_i}} f_{X_i}(x_i) \int_{D_Y} |f_Y(y) - f_{Y|X_i}(y|x_i)| dy dx_i \tag{5}$$

where $f_Y(y)$ is the unconditional probability density function (PDF) of the output $Y$ and $f_{Y|X_i}(y|x_i)$ is the conditional PDF given $X_i = x_i$. The integral $\int_{D_Y} |f_Y(y) - f_{Y|X_i}(y|x_i)| dy$ represents the distribution difference, and the final index is obtained by taking the expectation over the domain $D_{X_i}$ of $X_i$.

The classical Borgonovo index requires a large number of Monte Carlo simulations. Each time an input variable is fixed, the model needs to be rerun, which is computationally expensive, which is infeasible for high-dimensional or complex models. When combined with PCE, the

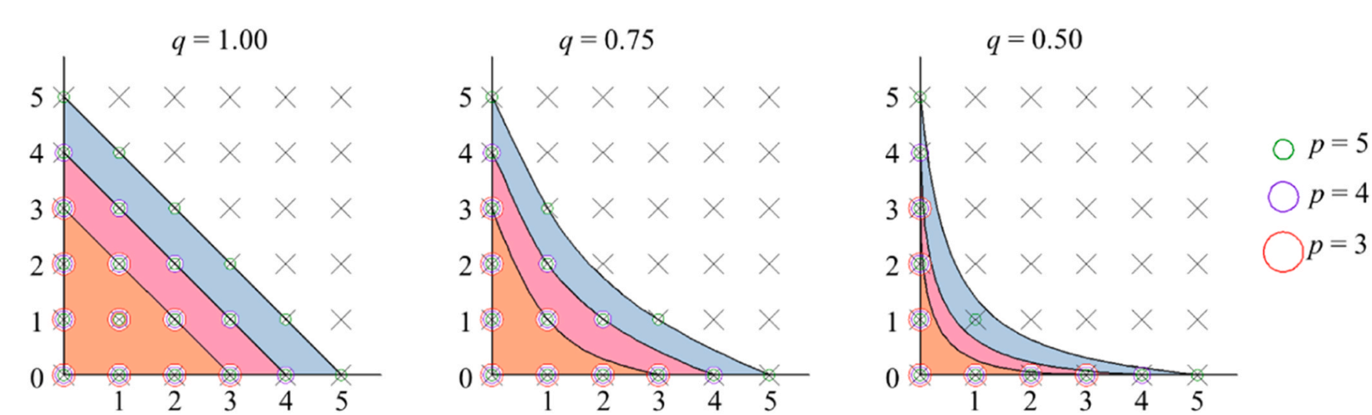


Fig. 1. Hyperbolic truncation set of $p$ and $q$ - adopted from [44].

number of model calls can be reduced, thus improving efficiency. At the same time, PCE can approximate complex functional relationships, providing more accurate conditional distribution estimates for the Borgonovo index.

When fixing $X_i = x_i^*$, the conditional response $\mathscr{M}^{PCE|X_i}(X_{-i})$ is obtained by analytically updating the PCE coefficients to exclude the correlation of $X_i$. Based on the established PCE model, Kernel Density Estimation (KDE) or the histogram method is used to generate conditional samples, and then $f_{Y|X_i}(y|x_i^*)$ is estimated.

For distribution difference calculation, the integral is approximated by the histogram binning method:

$$\int |f_Y(y) - f_{Y|X_i}(y|x_i^*)|dy \approx \sum_{b=1}^{B} |\hat{f}_Y(b) - \hat{f}_{Y|X_i}(b|x_i^*)|\Delta y \tag{6}$$

where $\hat{f}_Y$ and $\hat{f}_{Y|X_i}$are histogram-based estimates over bins $b$, and $\Delta y$ is the bin width. The outer integral is computed via Gaussian quadrature over $X_i$'s domain.

### 2.3. Bayesian inference

Bayesian Inference (BI) can update parameter estimates using prior information and observed data. This method is widely applied in various fields such as engineering, physics, and data analysis. It is particularly effective when solving inverse problems that require inferring model input parameters from indirect measurement data [49–51]. Bayesian inference combines the prior distribution and the likelihood function through Bayes' theorem to calculate the posterior distribution, as shown in Eq. (7):

$$\pi(X|Y) = \frac{L(X;Y)\pi(X)}{Z} \tag{7}$$

where $X$ is the parameter to be estimated, $Y$ is the observed data, $L(X;Y)$ is the likelihood function that describes the probability of the data under different parameter values, $\pi(X)$ is the prior distribution of the parameter, and $Z$ is the normalization factor, ensuring that the integral of the posterior distribution equals 1.

In practical applications, the posterior distribution of Bayesian inference usually does not have an analytical solution, so numerical methods are required. In this study, Markov chain Monte Carlo (MCMC) simulation is adopted to address this issue. The MCMC method constructs a Markov chain and uses sampling techniques to generate a sample sequence, making the stationary distribution of the chain consistent with the target posterior distribution. In this way, samples can be effectively drawn from the complex posterior distribution for parameter estimation, which has significant advantages when dealing with high-dimensional and complex posterior distributions [52].

Let the current state be $x^{(t)}$ and the next state be $x^{(t+1)}$. The transition between these two states is determined by the transition probability $K(x^{(t+1)}|x^{(t)})$. When the transition probability satisfies the detailed balance condition, the posterior distribution is the stationary distribution of the Markov chain:

$$\pi(x^{(t)}|Y)K(x^{(t+1)}|x^{(t)}) = \pi(x^{(t+1)}|Y)K(x^{(t)}|x^{(t+1)}) \tag{8}$$

Integrating Eq. (8), we can obtain:

$$\pi(x^{(t+1)}|Y) = \int_{\mathbb{R}^M} \pi(x^{(t)}|Y)K(x^{(t+1)}|x^{(t)})dx^{(t)} \tag{9}$$

Eq. (9) indicates that the posterior distribution remains unchanged during the transition process. Through ergodicity, the sample mean of the chain can approximate the posterior expectation as:

$$\mathbb{E}[h(X)|Y] \approx \frac{1}{T}\sum_{t=1}^{T} h(x^{(t)}) \tag{10}$$

where $T$ is the total number of iteration steps, and $h(x)$ is an arbitrary integrable function of the parameter $x$, which is used to calculate the expected value under the posterior distribution.

The Bayesian inference adopted in this study constructs a Markov chain to make its stationary distribution consistent with the target distribution, thereby indirectly sampling from the target distribution.

## 3. Proposed parameter identification method: PCE-BI

### 3.1. Process description

The PCE-BI method proposed in this section aims to use the PCE model to replace the high-cost FEA of footbridges, and combine Bayesian inference for identifying unknown material parameters of structures. The process is specified as follows:

**Step A:** Problem definition and prior setting

Construct a high-precision FE model that can fully reflect the structural characteristics of the research object. Select some input parameters that have a significant impact on the structural response as the unknown parameters to be identified, and set appropriate prior distributions.

**Step B:** Generate the initial dataset

Use the LHS method to generate multiple groups of input datasets for the FE model. Perform probabilistic FEA to extract the corresponding model output response datasets, and construct an initial dataset based on "input-output".

**Step C**：Construction and evaluation of the PCE model

Use 70 % of the initial dataset as the training set to construct the PCE model, and use the remaining 30 % as the validation set to evaluate the prediction performance of the PCE model. The adopted error evaluation index is the Leave-One-Out (LOO) cross-validation error, denoted as $Err_{LOO}$. If the prediction accuracy of the PCE model is reliable, output the model as a surrogate model for the FE model; otherwise, return to Step B to regenerate the initial dataset. In civil and structural engineering application scenarios, $Err_{LOO}$ ＜5E-2 is commonly considered an acceptable tolerance error.

**Step D**：PCE-driven accelerated Bayesian inference

Replace the time-consuming FEA directly with a high-precision PCE model to quickly generate structural response predictions. Integrate the structural response output predicted by the PCE and the measured structural response output into the objective function. Utilize the high efficiency of PCE, i.e. low computational cost and high prediction accuracy, to accelerate Bayesian inference, directly bypassing the high-cost FEA process, providing technical support for improving both computational efficiency and accuracy in subsequent parameter identification.

**Step E**：Parameter identification and model updating

Based on the posterior distribution generated by PCE-accelerated Bayesian inference, infer the optimal input parameters to complete the identification of unknown structural parameters. Substitute the identified parameters into the structural FE model to complete the model parameter update. By comparing the structural responses before and after the update, verify the updated model's ability to accurately map the performance of the actual structure.

After detailing the six core steps of the PCE-BI method, it is necessary to further clarify its inherent characteristics and implementation challenges. The PCE-BI method features two key characteristics. First, it constructs a lightweight, high - precision PCE surrogate model to replace the time consuming FE model, avoiding repeated calls. Second, it integrates Bayesian inference to account for material uncertainties, enabling efficient and accurate structural parameter identification via PCE -driven Bayesian inference. Its solving difficulties mainly lie in establishing a reasonable initial dataset and selecting appropriate PCE parameters, e.g., polynomial degree and truncation norm, to ensure model precision, as well as setting suitable computational parameters, e.g., number of chains and iterations, for effective sampling of high-dimensional parameter spaces in Bayesian inference.

A comprehensive flowchart outlining the PCE-BI method is presented

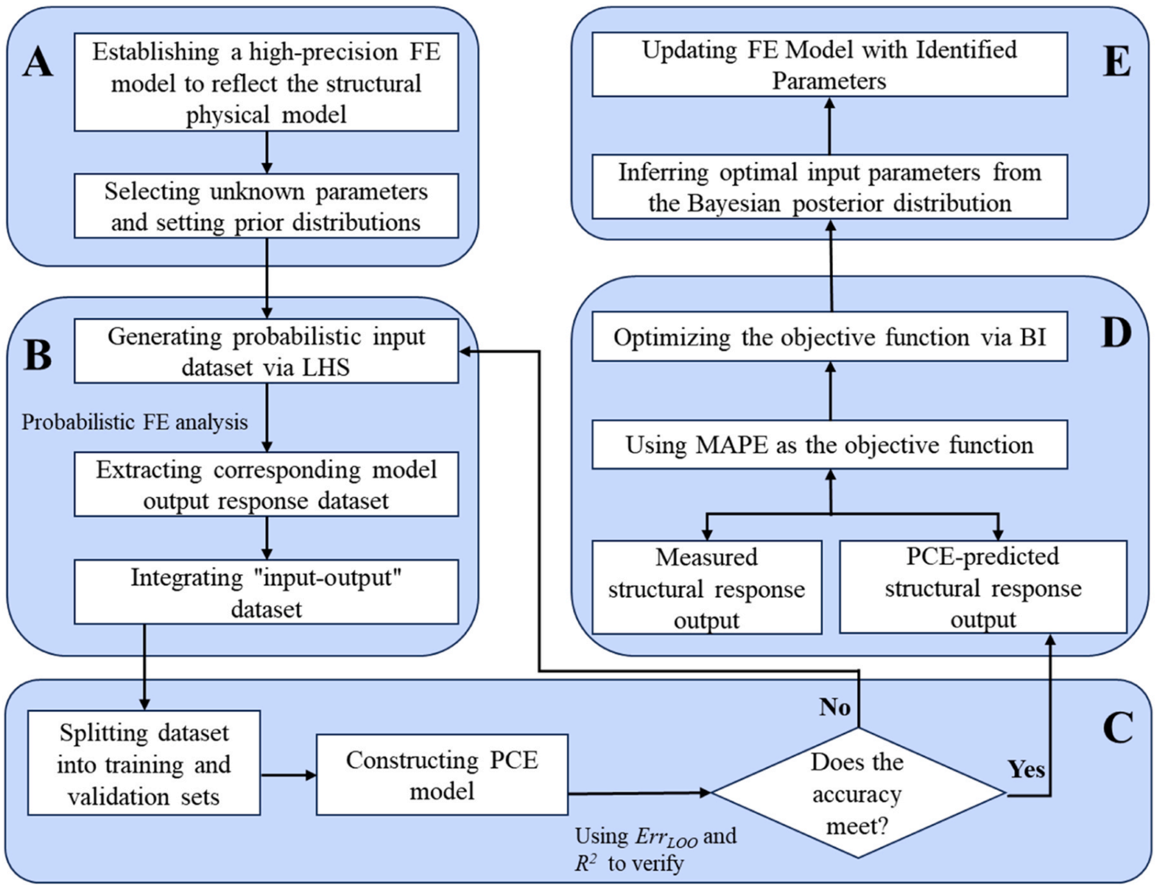


**Fig. 2.** Flowchart of the PCE-BI method.

in Fig. 2.

In this study, the construction of surrogate models including PCE were all completed using the open-source software UQLab. The numerical computing environment was based on a computer equipped with 16 GB of RAM and an i7 processor at 2.6 GHz. Probabilistic FEA was performed in Midas Gen, while the coupling of the PCE model and the BI was implemented in MATLAB.

### 3.2. Error validation metrics

First, the LOO cross-validation error is used to evaluate the predictive accuracy of the PCE model, and its equation is as follows:

$$Err_{LOO} = \frac{\sum_{i=1}^{N}\left(\mathscr{M}(\boldsymbol{x}^{(i)}) - \mathscr{M}^{PCE/i}(\boldsymbol{x}^{(i)})\right)^2}{\sum_{i=1}^{N}\left(\mathscr{M}(\boldsymbol{x}^{(i)}) - \hat{\mu}_Y\right)^2} \tag{11}$$

where $\mathscr{M}^{PCE/i}(\cdot)$ is the PCE model generated by excluding the $i^{th}$ sample point from the complete experimental design, and $\hat{\mu}_Y$ is the sample mean of the experimental design response, calculated as $\hat{\mu}_Y = \frac{1}{N}\sum_{i=1}^{N}\mathscr{M}(\boldsymbol{x}^{(i)})$.

The LOO cross-validation error serves as an indicator to evaluate model generalization via cross-validation. It mitigates over-fitting by iteratively excluding one sample point, creating a PCE model from the remaining samples, and computing the model's prediction error at the excluded point [35]. This approach avoids costly additional model evaluations for validation set construction. A smaller LOO cross-validation error signifies superior predictive performance of the PCE model, reflecting closer alignment between its outputs and those of the true model.

To more comprehensively evaluate the prediction performance of the surrogate model, the R-squared ($R^2$) value is used to assess the degree of fit of the prediction model to the data. The calculation equation is as follows:

$$R^2 = 1 - \frac{\sum_{i=1}^{n}\left(y_{true,i} - y_{PCE,i}\right)^2}{\sum_{i=1}^{n}\left(y_{true,i} - \overline{y}_{true}\right)^2} \in [0,1] \tag{12}$$

where $y_{true,i}$ is the actual output value of the structural response in the validation dataset, $y_{PCE,i}$ is the predicted value of the PCE model corresponding to $y_{true,i}$, and $\overline{y}_{true}$ is the mean of the output values in the validation dataset.

The $R^2$ value ranges between 0 and 1. A value closer to 1 indicates a better fit of the model to the data, meaning smaller prediction errors. Conversely, a value closer to 0 suggests a poorer fit.

Secondly, Gelman-Rubin diagnostics is selected to assess the convergence of MCMC simulations in Bayesian inference. Its basic idea is that if the parallel Markov chains have converged, then the within-chain variance and the between-chain variance should be similar. The expression is as follows:

$$R^p = \sqrt{\frac{g-1}{g} + \frac{q+1}{q \cdot g}\frac{B}{W}} \tag{13}$$

where $q$ is the number of Markov chains, $g$ is the length of each Markov chain, $B$ is the between-chain variance, which is the variance among the means of different Markov chains, and $W$ is the within-chain variance, which is the average of the variances within each Markov chain.

As the Markov chain converges, $R^p$ will approach 1. According to the recommendations of Gelman and Rubin, for most situations, when

$R^p < 1.2$, in such complex systems, it can balance "computational efficiency" and "result reliability", avoiding sampling bias caused by an overly loose threshold while reducing redundant calculations through multi-chain collaborative exploration. Therefore, the threshold of $R^p < 1.2$ is reasonable choice for structural parameter identification in this study [36].

Finally, the Mean Absolute Percentage Error (MAPE) is selected to evaluate the parameter identification accuracy of the PCE-BI method. Its definition is as follows:

$$MAPE = \frac{100\%}{n}\sum_{i=1}^{n}\frac{|y_{T,i} - y_{PB,i}|}{y_{T,i}} \tag{14}$$

where $y_{T,i}$ is the actual measured or calculated value of the structure response, $y_{PB,i}$ is the predictive value based on the PCE model, and $n$ is the number of fitted points.

MAPE provides an intuitive percentage-based measure of error. A lower MAPE value indicates higher accuracy of the PCE-BI method.

## 4. Construction of PCE model for curved footbridge

### 4.1. Numerical model

A glass-enclosed sightseeing footbridge is built on top of a commercial complex. This footbridge is curved, with a total length of 59.6 m, a width of approximately 7 m, a maximum overhang of 28.5 m, and a total mass of 2398.36 tons. The main structural components of the curved footbridge are made of Q390 steel trusses. The two sides and the top are enclosed by glass. The two side spans and the two ends of the main span are paved with C35 concrete decks, while the middle of the main span features a glass deck.

During structural design, the objective was to maximize the

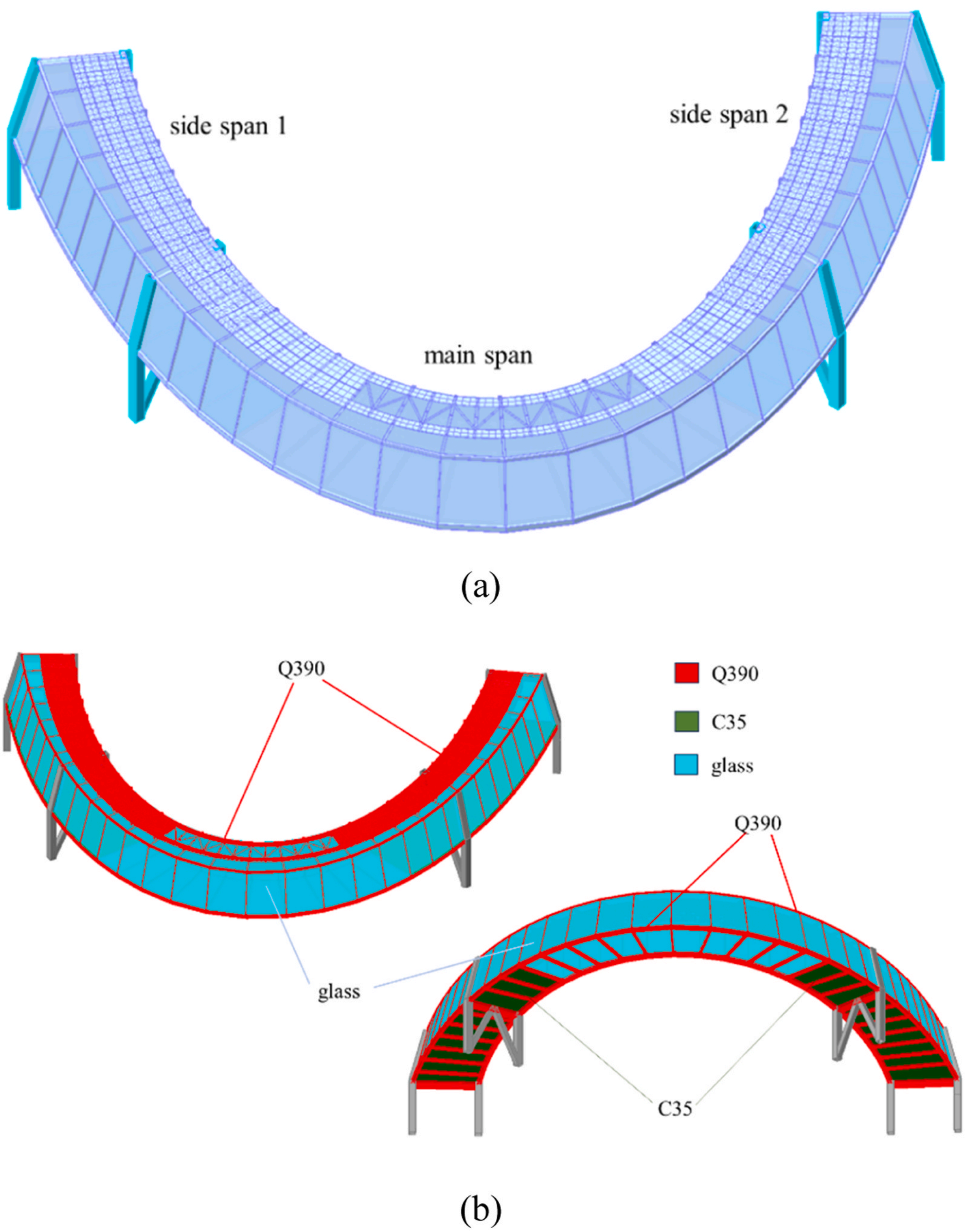


**Fig. 3.** Description of curved footbridge: (a) Numerical model and (b) three material zones.

frequency. After topology analysis and optimization of the members, the horizontal frequency is above 3.24 Hz, which is outside the comfort-sensitive frequency range. However, the vertical frequency is 2.16 Hz, still within the comfort-sensitive range, necessitating a human-induced vibration floor comfort analysis. To more accurately represent the actual structural response, a high-precision FE model of the footbridge was constructed using Midas Gen software, encompassing the main structure of the footbridge and its supporting columns, as shown in Fig. 3(a). The three material zones of the footbridge body are depicted in Fig. 3(b), and the material properties are specified according to design codes, as shown in Table 1.

The force exerted by pedestrians on the footbridge structure adopts the continuous walking load model recommended by IABSE [53], and the equation of this model is shown in Eq. (15):

$$F_p(t) = G\left[1 + \sum_{i=1}^{n} \alpha_i \sin\left(2i\pi f_p - \Phi_i\right)\right] \tag{15}$$

where $G$ is the weight of a single pedestrian, taken as 0.7 kN, $f_p$ is the pedestrian's stepping frequency, $\alpha_i$ is the $i$-th order dynamic load factor. Since the high-order load frequencies contribute little to the structural vibration, and the first three orders can meet the requirements, $\alpha_1 = 0.4 + 0.25\left(f_p - 1\right)$, $\alpha_2 = \alpha_3 = 1.0$, $\Phi_i$ is the $i$-th order phase angle, $\Phi_1 = 0$, $\Phi_2 = \Phi_3 = \pi/2$.

According to the use of the footbridge, the pedestrian traffic density is taken as 1 pedestrian/m$^2$, and the pedestrian stepping frequency is taken as 2 Hz. The number of pedestrians on the structure is equivalent to the number of people walking in synchrony [54], and the calculation equation is as follows:

$$N_e = 1.85\sqrt{N}\left(\text{density} \geqq 1\mathrm{P}\Big/\mathrm{m}^2\right) \tag{16}$$

where $N_e$ is the equivalent number of people, $N$ is the number of pedestrians on the structure, and P represents pedestrian.

The crowd load is applied to the deck of the footbridge structure in the form of nodal dynamic loads. Dynamic calculations are carried out on the footbridge structure according to the continuous walking load model. The vertical acceleration distribution of the deck is shown in Fig. 4. It can be seen from Fig. 4 that the acceleration distribution of the footbridge deck forms three peak regions. The acceleration peak of each span deck occurs at the outer-side nodes in the middle of the span, and the acceleration peak of all bridge nodes occurs at the outer-side of the middle area of main-span. Thus, the vertical vibration of the footbridge in the mid-span area is of the greatest concern. Therefore, 6 nodes on the inner and outer sides of the mid-span of each span are selected as observation points, and the acceleration peaks of these 6 measurement points are taken as the QoIs.

### 4.2. Construction of prior distribution parameter space

Considering that the Poisson's ratio and the coefficient of linear thermal expansion have little effect on the vertical acceleration of the structure [55,56], the parameters to be identified in this study are the elastic modulus and densities of the three material zones of the footbridge body, a total of 6 unknown input parameters. Considering that material parameters usually have inherent random characteristics, it is assumed that these parameters to be identified all follow a common Gaussian distribution model [24,57]. The values in Table 1 are taken as the means of the probability distribution model, and a standard deviation of 5 % is given for Q390 steel and glass, and 10 % for C35 concrete. Table 2 presents the prior distributions and statistical values of the 6 unknown input parameters.

**Table 1**
Material properties for curved footbridge.

| Component Name | Elastic modulus [MPa] | Density [kg/m$^3$] | Poisson's ratio [-] | Coefficient of linear Thermal expansion [1/℃] |
|---|---|---|---|---|
| Q390 Steel | $2.06 \times 10^5$ | $7.85 \times 10^3$ | 0.3 | $1.2 \times 10^{-5}$ |
| C35 Concrete | $3.15 \times 10^4$ | $2.4 \times 10^3$ | 0.2 | $1 \times 10^{-5}$ |
| Glass | $7.2 \times 10^4$ | $2.611 \times 10^3$ | 0.2 | $0.8 \times 10^{-5}$ |

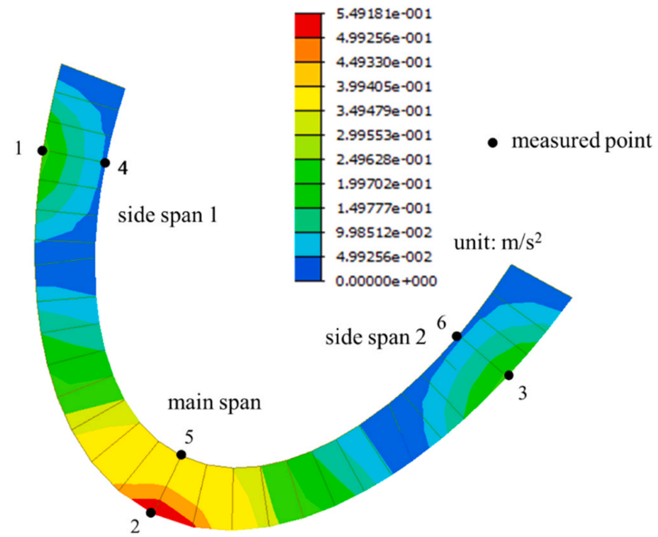


**Fig. 4.** Vertical acceleration distribution on the footbridge floor.

### 4.3. PCE model

For the 6 unknown input parameters in Table 2, the LHS method is used to conduct 50 random samplings. These samples are then substituted into the FE model of the footbridge for dynamic calculations. The acceleration peaks at the selected measuring points are extracted as QoIs, thereby generating 50 sets of "input-output" datasets as the initial dataset for constructing the surrogate model. Among them, the first 35 sets are used as the training set for constructing the PCE model, and the last 15 sets of data are used as the validation set to evaluate the prediction accuracy of the PCE model.

To explore the influence of different truncation schemes and polynomial degrees on the accuracy of the PCE model, this study considers truncation norms $q = [1.0, 0.75, 0.5]$ and polynomial degrees $p = [1,2,3,4,5,6,7,8,9,10]$, and a total of 180 PCE models are constructed. Fig. 5 shows the accuracy of all PCE models, and the following conclusions can be drawn:

- The polynomial degree $p$ is a key factor affecting the accuracy of the PCE model. When $p < 5$, the low dimensionality of the basis function

**Table 2**
Unknown parameter probabilistic input priori model for curved footbridge.

| Component Name | Unknown Parameters | Symbol | Model | Quantity |
|---|---|---|---|---|
| Q390 Steel | Elastic modulus | $E1$ | Gaussian | N($2.06 \times 10^5$, $1.03 \times 10^4$) |
| | Density | $D1$ | Gaussian | N($7.85 \times 10^3$,$3.925 \times 10^2$) |
| C35 Concrete | Elastic modulus | $E2$ | Gaussian | N($3.15 \times 10^4$, $3.15 \times 10^3$) |
| | Density | $D2$ | Gaussian | N($2.4 \times 10^3$, $2.4 \times 10^2$) |
| Glass | Elastic modulus | $E3$ | Gaussian | N($7.2 \times 10^4$,$3.6 \times 10^3$) |
| | Density | $D3$ | Gaussian | N($2.611 \times 10^3$,$1.306 \times 10^2$) |

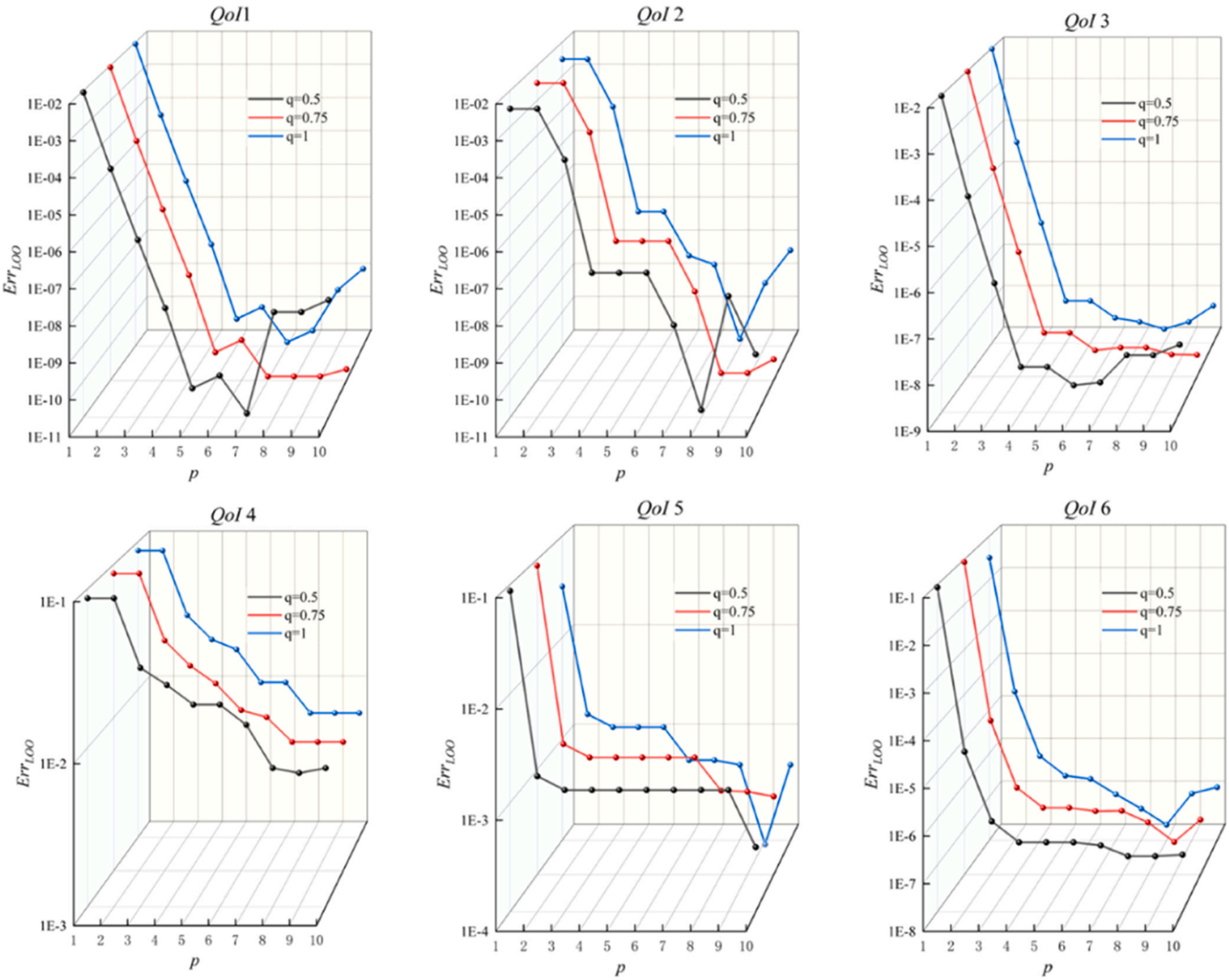


**Fig. 5.** Quantification of $Err_{LOO}$ for the curved footbridge based on the PCE model.

space leads to model underfitting, and the accuracy increases significantly with the increase of $p$. When $p > 5$, the basis function has sufficient nonlinear expression ability, and the accuracy improvement tends to level off, with divergence due to different QoIs.

- The truncation norm $q$ affects the accuracy through basis function screening strategies. When $q = 0.75$, the middle and high order core basis functions are preferentially retained to suppress overfitting, enabling high order polynomials to achieve both high accuracy and robustness. When $q = 0.5$, low order basis functions are prioritized for screening, allowing efficient and accurate fitting through simple basis function combinations under low-order polynomials.

Therefore, based on the collaborative optimization analysis of the polynomial degree and the truncation norm, a unified set of parameters $q = 0.75$ and $p = 5$ is adopted to construct an overall PCE model that includes 6 QoIs to characterize the structural response of the curved footbridge. The choice of a unified model over QoI-specific models is primarily to ensure that the overall prediction accuracy meets engineering requirements, while significantly reducing the computational complexity of model construction and subsequent PCE-BI method. This avoids redundancy from maintaining multiple models and provides more efficient technical support for multi-parameter identification of the footbridge.

Moreover, to further verify the global fitting ability of the PCE model, the $R^2$ coefficient is introduced for evaluation. As shown in Fig. 6, the $R^2$ value reaches 0.99946, further indicating that the PCE model has excellent prediction performance.

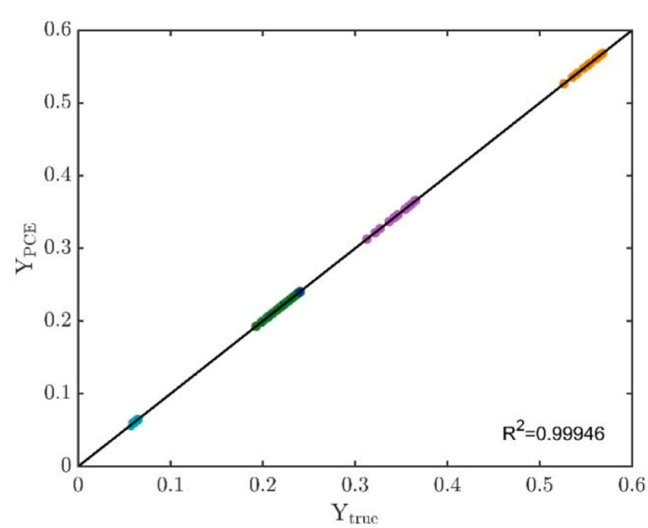


**Fig. 6.** The prediction accuracy of PCE model.

It is worth noting that this study primarily focuses on the vibration response of pedestrian bridges under pedestrian loading, during which the material deformation remains within the linear elastic range, and the model response is smooth, differentiable, and continuous. In addition, the material parameters exhibit inherent randomness and follow certain probability distributions, with a relatively low input dimensionality. These conditions are particularly well-suited for PCE model construction. However, the generalization ability of the PCE model under other loading scenarios remains to be verified.

*4.3.1. PCE-based Borgonovo indices for sensitivity analysis*

Based on the constructed lightweight and reliable PCE model, a Borgonovo indices-based sensitivity analysis was conducted on the input parameters of the footbridge, To clarify the regulatory mechanism of input parameters on the dynamic response of the curved footbridge and support structural parameter optimization and vibration-reduction design, the focus was on exploring the impact of 6 input parameters on the acceleration peaks (QoI1–3) at three measuring points in the outer of mid-span in Fig. 4. The results of the sensitivity analysis are shown in Fig. 7, and the observations are as follows:

- The acceleration peaks at the side spans (QoI1 and QoI3) are highly sensitive to D1, as indicated by the high sensitivity indices and strong negative correlation. Since the side spans are mainly made of steel, increasing the steel density shifts the natural frequency away from the excitation frequency, thereby reducing resonance and effectively suppressing vibration.
- The acceleration peak at the main span (QoI2) is most sensitive to D3, as reflected by the strong negative correlation. As glass is the primary material of the main span, increasing its density shifts the natural frequency away from the excitation frequency, thus reducing resonance and effectively suppressing vibration.

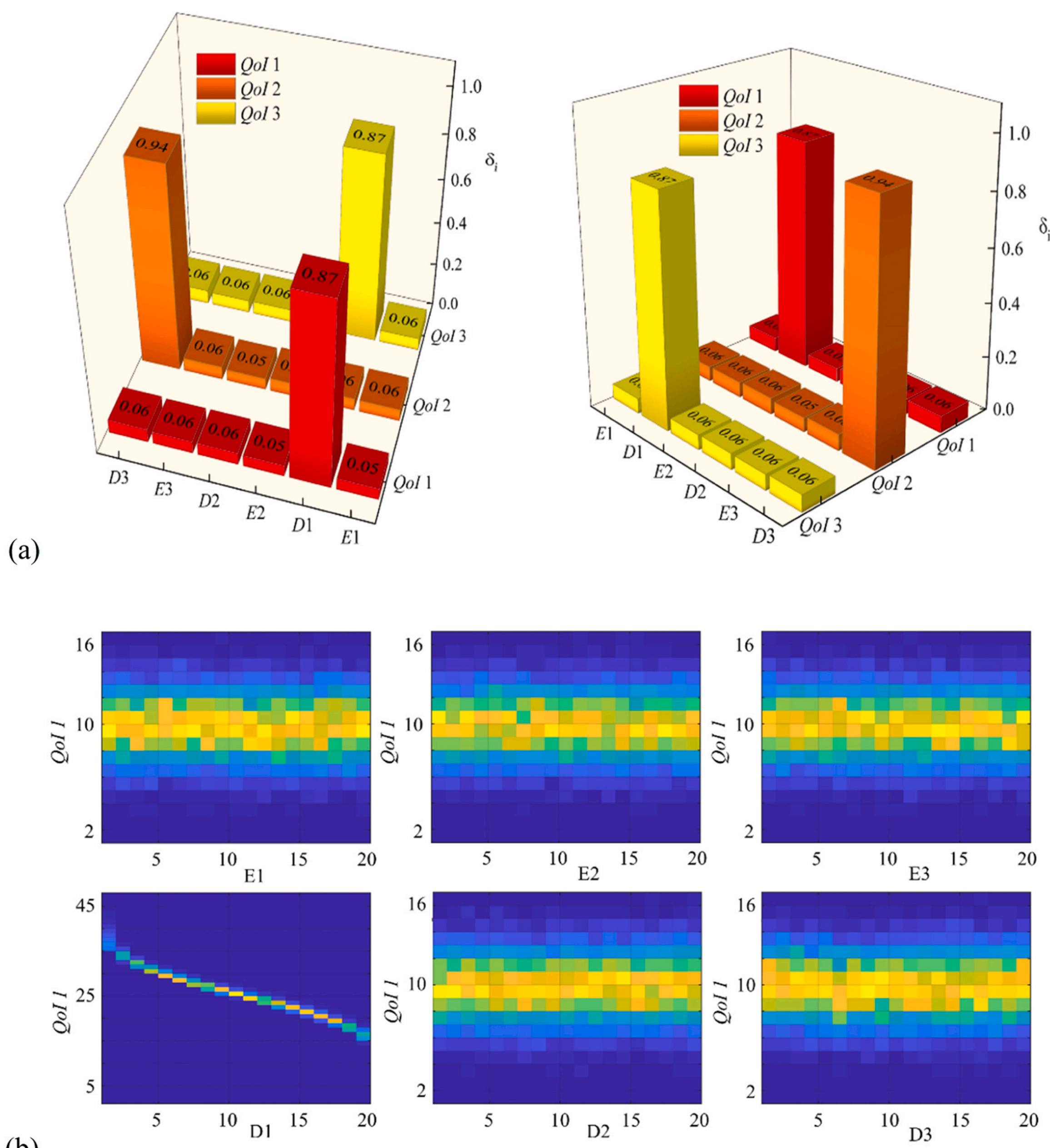


**Fig. 7.** PCE-based Borgonovo' indices sensitivity analysis: (a) PCE-based Borgonovo' indices for QoI1–3: 3D Visualizations from Dual Perspectives, and (b)-(d) Histogram estimate of the joint PDF of input parameters and QoI1–3.

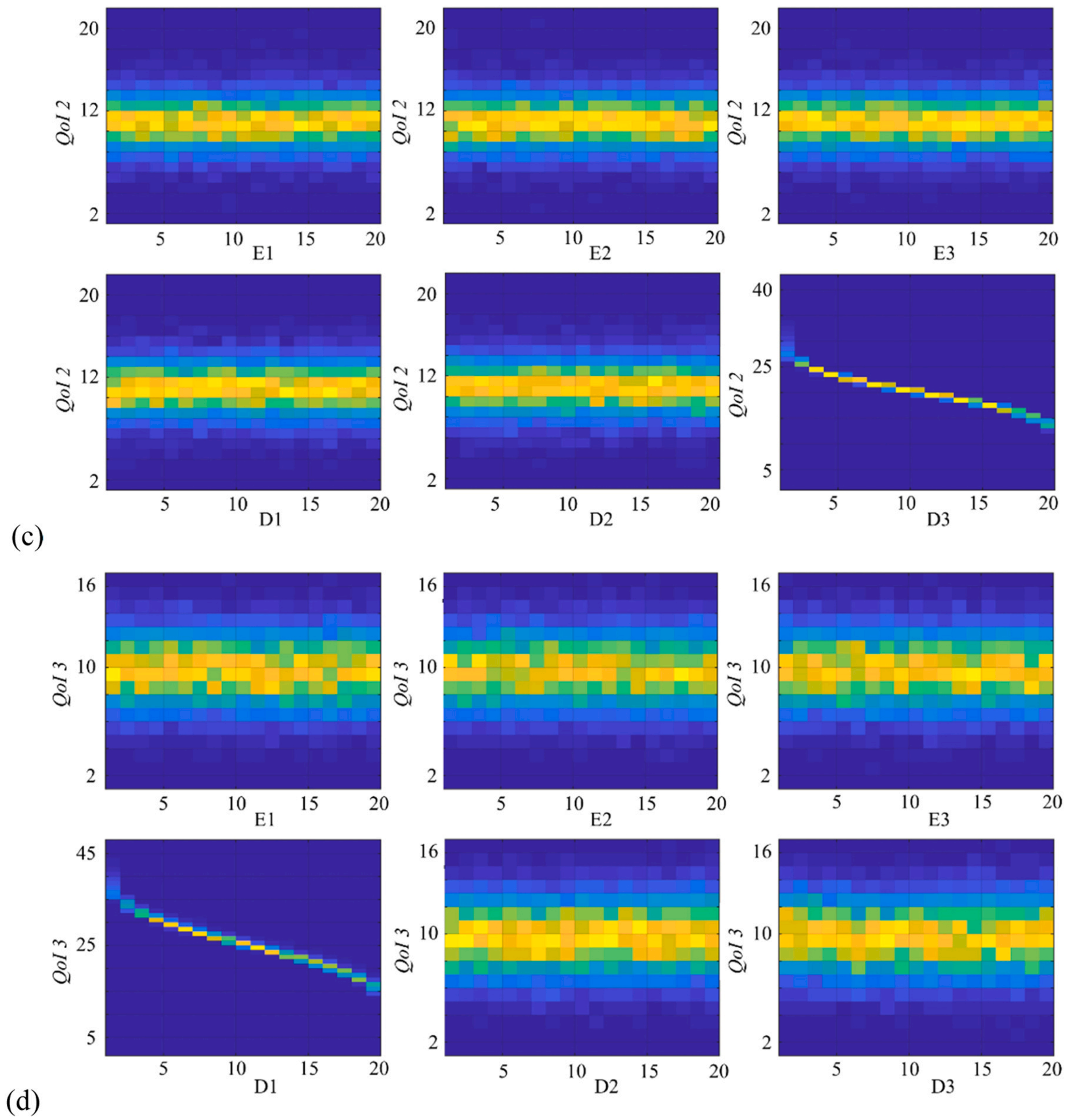


**Fig. 7.** (*continued*).

- The elastic modulus of the three materials has little effect on the acceleration peaks, as indicated by the low sensitivity indices. This suggests that modifications to material stiffness without corresponding changes in structural configuration or mass are insufficient to effectively reduce vertical vibrations. Instead, mass distribution remains the dominant factor influencing vibration control.

Notably, for Fig. 7(b)-(d), different colors represent the relative magnitude of joint probability density, where warmer colors (e.g., yellow) indicate higher joint probability density of the input-output combinations, while cooler colors (e.g., blue) indicate lower joint probability density.

It is worth noting that the observed phenomenon in this study, where density parameters (D1, D3) dominate over elastic moduli in influencing vibration responses, is closely related to the dynamic characteristics of this long-span curved footbridge. This bridge is a flexible structure with a natural frequency close to pedestrian's stepping frequency, and under pedestrian load excitation, its vertical vibration response is dominated by near-resonance. The mass distribution of this bridge directly affects its natural frequency, making density a key factor. This scenario may be applicable to other flexible footbridges with vertical frequencies in the comfort-sensitive range, but it is not a universal principle. For footbridges with higher stiffness, the influence of elastic modulus on vibration responses may be more prominent. Therefore, the relative importance of density and elastic modulus depends on the structural dynamic characteristics and external excitation features, and specific analysis is required for other structures.

### 4.4. Kriging and SVR model

To highlight the superiority of the PCE model, it is compared with the popular Kriging model and SVR model. To ensure the fairness of the comparison, the initial datasets required for constructing the surrogate models are all the same. In addition, both the Kriging model and the SVR model adopt the Genetic Algorithm (GA) for hyperparameter optimization. Fig. 8 presents the comparison results of the prediction accuracy and efficiency of the three surrogate models, and the conclusions are as follows:

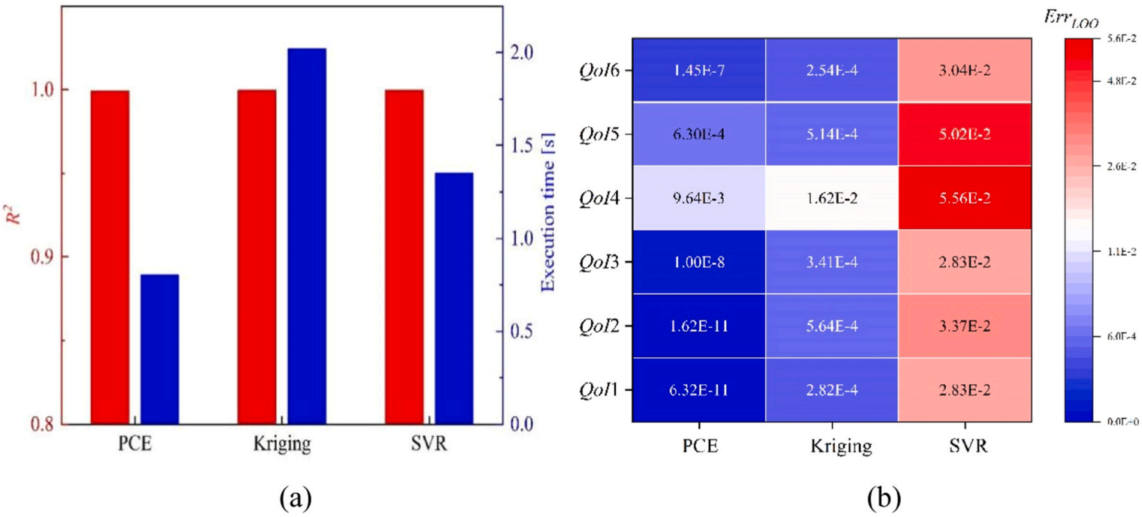


**Fig. 8.** Comparison of the prediction efficiency and accuracy of three surrogate models: (a) R-squared values and execution time of three models, and (b) $Err_{LOO}$ for the three models.

- In terms of prediction accuracy, the $R^2$ values of the three surrogate models are all very close to 1, indicating that they all have excellent prediction capabilities for the footbridge response; the LOO error of the PCE model is significantly lower than that of the Kriging and SVR models, indicating that the PCE model has a better fitting accuracy for high-dimensional nonlinear responses.
- Regarding computational efficiency, the execution time of the PCE model is only 1/3 of that of the Kriging model and 1/2 of that of the SVR model. This shows that when dealing with multiple QoIs, the PCE model has a significant efficiency advantage. Compared with the other two surrogate models that rely on hyperparameter optimization, the PCE model can bypass the complex hyperparameter optimization process, reducing computational time while ensuring high prediction accuracy, and better balancing prediction accuracy and computational efficiency.

From the above analysis, the PCE model is significantly superior to the Kriging and SVR models in both prediction accuracy and computational efficiency. It provides a lightweight and efficient technical solution for uncertainty quantification analysis of complex structures.

## 5. Parameter identification of curved footbridge

Section 4 has demonstrated the superior predictive performance of the PCE model. The PCE-BI method proposed in Section 3 will now be applied to identify the unknown material parameters of the footbridge. To highlight the efficiency superiority of the PCE-BI method in handling parameter identification problems, it is compared with traditional iterative optimization-based method. The traditional iterative optimization-based method directly combines Bayesian inference with the structural FE model, denoted as FEM-BI, which is implemented through joint simulation using MATLAB and Midas Gen. In addition, the coupling methods of the Kriging and SVR models with Bayesian inference are also included in the comparison, denoted as Kriging-BI and SVR-BI, to indirectly verify the advantages of the PCE model in dealing with uncertainty problems.

Considering the confidentiality restrictions of the ongoing project, it is difficult to obtain the measured response data at the measuring points of the footbridge. To verify the effectiveness and practicality of the proposed method, this work adopts a substitute scheme of "FE model + virtual measuring point simulation data". Specifically, based on the high-precision FE model of the footbridge, the acceleration peaks are extracted at the selected measuring point locations as the "virtual measured response" for testing, and 10 % uncertainty is introduced to simulate the measurement error in actual engineering, thereby enhancing the real-world relevance of the method verification. The "virtual measured response" is given by Eq. (17) [58]:

$$R_Y = \frac{\sum_{i=1}^{N} R_{FEM,i}}{N} \times (1 + 0.1R_n) \tag{17}$$

where $R_Y$ represents the virtual measured response, $R_{FEM,i}$ denotes the output result of the $i$-th FEA, $N$ represents the number of random samples used to construct the PCE model. As indicated in Section 4.3, $N$ is set to 50, and $R_n$ is a random matrix, and the value of each element is in the interval [0, 1].

Traditional Bayesian inference uses MCMC as a solver for parameter estimation. The number of chains and the number of iterations are the core factors affecting the calculation accuracy. For complex high-dimensional parameter models, a sufficient number of chains is required to ensure effective sampling of the high-dimensional parameter space [36,59], avoiding sampling bias caused by the curse of dimensionality. The determination of the number of iterations needs to be achieved through convergence assessment to ensure the validity of the posterior distribution. However, in the traditional FEM-BI method, since each iteration step requires calling the FE calculation response, it leads to a high frequency of FE calls and high computational costs.

In this study, for the FEM-BI method, solutions are obtained by setting different numbers of chains, and the Gelman-Rubin diagnostics is used to assess the convergence state. The first 200 steps are set as burn-in. The changes of $R^p$ values with the number of iterations under different numbers of chains are shown in Fig. 9, with a convergence threshold of 1.2. The following main conclusions can be drawn:

- When the number of chains is small, as the number of iterations increases, the $R^p$ value fluctuates relatively greatly and the convergence speed is slow, because a small number of chains cannot well cover the target distribution space, resulting in certain randomness and bias. As the number of chains increases, the fluctuation of the $R^p$ value decreases, and it can converge more quickly, indicating that increasing the number of chains is beneficial for exploring the target distribution and improving the convergence speed.
- When the number of chains is greater than 90 and the number of iterations exceeds 1100, $R^p$ fluctuates little and is stably lower than 1.2, indicating that the MCMC simulation has reached convergence, and the samples obtained at this time can be used for subsequent

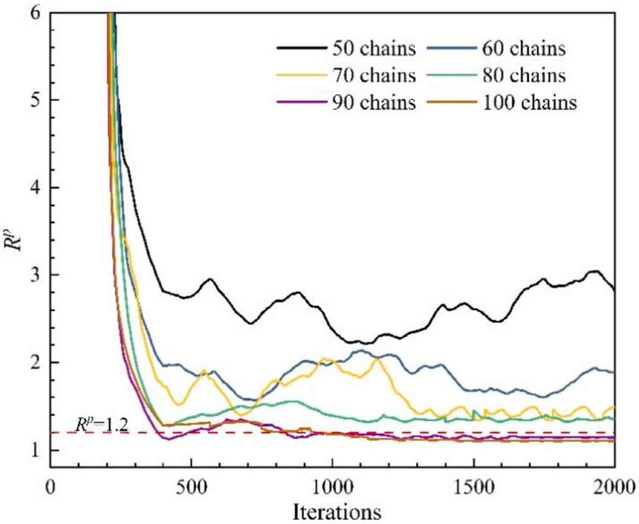


**Fig. 9.** Convergence of MCMC simulation in BI with different numbers of chains.

Bayesian inference analysis.

To further verify the convergence, after selecting the MCMC simulation parameters based on the Gelman-Rubin diagnostic conclusion, an analysis of the trace plots of six inversion parameters is carried out, as shown in Fig. 10. Some observations are as follow:

- As the number of iterations progresses, the parameter trace lines initially show fluctuations. However, all six parameters gradually stabilize after 1100 iterations. In the stable state, the parameter values are concentrated within a narrow range, which indicates that the MCMC chains have converged to a stationary distribution.
- This visualized result is consistent with the Gelman-Rubin diagnostic conclusion. It not only further confirms the rationality of the selection of calculation parameters but also firmly provides support for the reliability of structural parameter identification.

In summary, to ensure the accuracy of parameter inversion in the traditional Bayesian inference method, in the parameter identification of the curved footbridge, the number of chains and the number of iteration steps for the FEM-BI method are set to 90 and 1100 respectively, providing benchmark computational parameters for the subsequent comparison of multiple methods.

The total computational time of the method coupling the surrogate model with Bayesian inference in this study consists of two parts. The first part (Part 1) is the time to construct the "input-output" dataset for the surrogate model, with PCE-BI, Kriging-BI, and SVR-BI sharing an identical duration in this step as they rely on the same initial dataset. The second part (Part 2) encompasses both the training time of the surrogate models (PCE, Kriging, or SVR), and the running time of the coupled method within MATLAB for Bayesian inference (BI) using the pre-trained surrogate models.

The parameter identification results of the four methods are shown in Table 3, and the comparison results of computational accuracy and efficiency are summarized in Table 4 and Fig. 11. The following

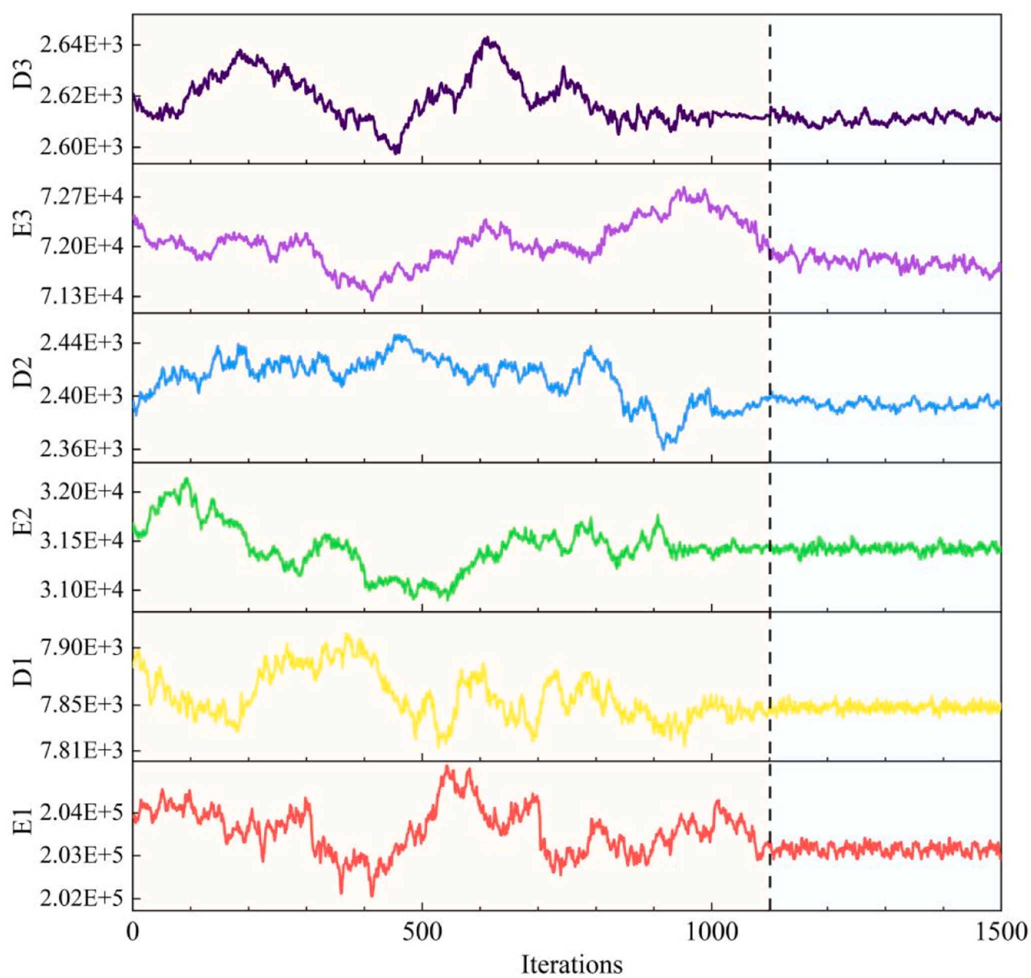


**Fig. 10.** The trace plots of six inversion parameters.

**Table 3**
Parameter identification results of four methods for curved footbridge.

| Method | PCE-BI | Kriging-BI | SVR-BI | FEM-BI |
|---|---|---|---|---|
| $E1$ | $2.052 \times 10^5$ | $2.054 \times 10^5$ | $2.058 \times 10^5$ | $2.032 \times 10^5$ |
| $D1$ | $7.771 \times 10^3$ | $7.798 \times 10^3$ | $7.827 \times 10^3$ | $7.848 \times 10^3$ |
| $E2$ | $3.145 \times 10^4$ | $3.120 \times 10^4$ | $3.094 \times 10^4$ | $3.142 \times 10^4$ |
| $D2$ | $2.318 \times 10^3$ | $2.351 \times 10^3$ | $2.338 \times 10^3$ | $2.399 \times 10^3$ |
| $E3$ | $7.006 \times 10^4$ | $7.186 \times 10^4$ | $7.131 \times 10^4$ | $7.183 \times 10^4$ |
| $D3$ | $2.505 \times 10^3$ | $2.590 \times 10^3$ | $2.596 \times 10^3$ | $2.613 \times 10^3$ |

**Table 4**
Comparison between the measured and predicted response for curved footbridge.

| Measured point | $R_Y$ [m/s$^2$] | PCE-BI | Kriging-BI | SVR-BI | FEM-BI |
|---|---|---|---|---|---|
| 1 | 0.234 | 0.222 | 0.221 | 0.221 | 0.219 |
| 2 | 0.569 | 0.558 | 0.552 | 0.550 | 0.547 |
| 3 | 0.229 | 0.215 | 0.214 | 0.214 | 0.213 |
| 4 | 0.063 | 0.061 | 0.061 | 0.061 | 0.060 |
| 5 | 0.366 | 0.347 | 0.340 | 0.339 | 0.337 |
| 6 | 0.064 | 0.062 | 0.061 | 0.061 | 0.060 |
| MAPE [%] | | 4.11 | 5.01 | 5.11 | 6.03 |
| Part 1 [hr] | | 3.351 | 3.351 | 3.351 | - |
| Part 2 [s] | | 79.69 | 382.73 | 218.66 | - |
| Total time [hr] | | 3.373 | 3.457 | 3.412 | 107.426 |

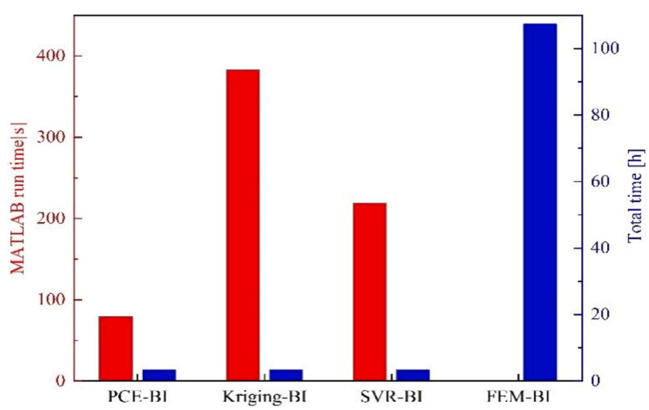


**Fig. 11.** Comparison of efficiency between four methods.

conclusions can be drawn:

- The adoption of the surrogate model improves the computational accuracy. Among them, the PCE-BI method has the best performance. Traditional FEM-BI, relying on MCMC sampling, accumulates errors in high-dimensional spaces. Surrogate models eliminate random FEM errors via pre-training. Moreover, PCE uses orthogonal polynomials for global parameter-response fitting, resisting local data fluctuations better than Kriging and SVR.
- Combining the surrogate model with Bayesian inference can significantly reduce the total computational time. Among them, the PCE-BI method takes the shortest time, with a total of 3.373 h. Compared with the 107.426 h of the FEM-BI method, the efficiency improves by 31.8 times. The PCE model eliminates the need to repeatedly invoke FEM analyses, thus avoiding the high computational expense inherent in the FEM-BI approach.
- A comparison of the PCE-BI, Kriging-BI, and SVR-BI methods reveals substantial differences in computational time for Part 2. The PCE-BI method is nearly three times faster than SVR-BI and five times faster than Kriging-BI, further demonstrating its significant efficiency advantage. This improvement is primarily attributed to the fact that PCE-BI does not require hyperparameter optimization.

It should be noted that the computational times reported in this study are hardware-dependent, but their scalability with respect to problem size can be described as follows:

- The complexity of constructing the PCE surrogate model can be characterized by the number of input parameters (M), polynomial basis size (P), and number of QoIs (K). When using Latin hypercube sampling, the number of samples grows linearly with M, corresponding to a complexity of O(M); under hyperbolic truncation, P grows polynomially with M, i.e., P = O(Mˆ$p$), where $p$ is the polynomial degree. Since a separate PCE model needs to be constructed for each QoI, the overall complexity is O(K·(M + P)).
- For the PCE-BI method, the cost per iteration is reduced from the high complexity of FEA (O(FEM)) to the low complexity of PCE evaluation (O(K·P)), where the complexity of FEA grows exponentially with problem size. Thus, the total complexity of PCE-BI is O (N + T·K·P), where T is the number of iterations. In contrast, the complexity of traditional FEM-BI is O(T·FEM), which is much higher than that of the PCE-BI method.

Overall, in terms of balancing computational accuracy and efficiency, the PCE-BI method demonstrates the most outstanding performance. To further assess the robustness of the PCE-BI method under different noise levels (i.e., measurement uncertainties), tests were conducted with noise levels of [5 %, 10 %, 15 %, 20 %]. The comparison results are shown in Table 5, from which it can be seen that the parameter identification performance of the PCE-BI method is only slightly affected by noise disturbances. This directly demonstrates that the proposed method possesses strong robustness and noise resistance.

## 6. Conclusion

Focusing on the human-induced vibration characteristics of curved pedestrian bridges, this study proposes the PCE-BI method. Through a lightweight surrogate model combined with a BI framework, efficient parameter identification is achieved in a complex parameter space. The main research conclusions are as follows:

- The PCE surrogate model is constructed based on 50 datasets generated by LHS. Evaluated by LOO cross-validation and the $R^2$ metric, its accuracy is significantly superior to Kriging and SVR models. Moreover, it does not require hyperparameter optimization and has higher computational efficiency. This high-accuracy model provides a reliable basis for PCE-BI-based multi-parameter identification.
- Sensitivity analysis shows that the acceleration peaks at the side spans are most sensitive to the density of Q390 steel (D1), while the main span is most sensitive to the density of glass (D3).
- Compared with Kriging-BI and SVR-BI, the PCE-BI method demonstrates superior accuracy and robustness. Its global analytical fitting capability avoids the local interpolation biases present in Kriging and SVR, resulting in more reliable and low-variance parameter estimates.
- Compared with the traditional FEM-BI method, all surrogate model driven approaches eliminate the need for repeated FEA, greatly improving computational efficiency. Among these methods, the PCE-BI method achieves the highest efficiency and accuracy, with a 31.8-fold improvement in computational speed and superior identification of the posterior distributions of six material parameters for the curved footbridge compared to FEM-BI. These results fully demonstrate the outstanding applicability and reliability of the PCE-BI method in engineering practice.

In summary, the PCE-BI method proposed in this study effectively overcomes the deficiencies of traditional parameter identification methods in terms of computational accuracy and efficiency. It is

**Table 5**
Comparison between the measured and predicted response under different noise levels based on the PCE-BI method.

| Measured point | $R_Y$ [m/s$^2$] 5 % noise | PCE-BI | $R_Y$ [m/s$^2$] 10 % noise | PCE-BI | $R_Y$ [m/s$^2$] 15 % noise | PCE-BI | $R_Y$ [m/s$^2$] 20 % noise | PCE-BI |
|---|---|---|---|---|---|---|---|---|
| 1 | 0.229 | 0.220 | 0.234 | 0.222 | 0.251 | 0.239 | 0.259 | 0.244 |
| 2 | 0.564 | 0.550 | 0.569 | 0.558 | 0.601 | 0.576 | 0.642 | 0.598 |
| 3 | 0.223 | 0.213 | 0.229 | 0.215 | 0.244 | 0.231 | 0.219 | 0.217 |
| 4 | 0.062 | 0.060 | 0.063 | 0.061 | 0.062 | 0.061 | 0.061 | 0.061 |
| 5 | 0.356 | 0.341 | 0.366 | 0.347 | 0.390 | 0.371 | 0.406 | 0.383 |
| 6 | 0.063 | 0.060 | 0.064 | 0.062 | 0.067 | 0.064 | 0.072 | 0.065 |
| MAPE [%] | | 3.85 | | 4.11 | | 4.21 | | 4.82 |

applicable to the multi-parameter identification of complex long-span structures with uncertain material properties. This method can also be extended to other similar structures, providing reliable data support for the health monitoring, damage identification, and vibration control of long-span structures. However, this method has some limitations and deficiencies:

- Although the PCE model is a powerful regression modeling tool, its limitations were not fully discussed in this study. The PCE model is suitable for predicting the response of continuous material structures without abrupt changes or discontinuities. However, it may not applicable to these scenarios, such as strongly nonlinear systems, structural instability, etc. Moreover, it is inherently unsuitable for time series modeling.
- Constructing a surrogate model requires running the initial FE model multiple times, and the computational cost is limited by the complexity of the original model and the number of calculations. In this study, the current PCE-BI validation is restricted to a 2 Hz pedestrian's stepping frequency (near-resonance condition). Expanding verification to other loading scenarios would aggravate computational burdens, limiting generalization under diverse conditions currently due to computational constraints.
- The dynamic influence of the time-varying characteristics of material parameters on the structural response has not been considered.
- The current noise sensitivity analysis simplifies measurement errors as Gaussian and uniform, which may not fully reflect real-world scenarios. Non-Gaussian noise could increase the dispersion of posterior parameter distributions and reduce identification stability.

Future research can be deepened in the following directions:

- Explore approaches for constructing accurate surrogate models using fewer initial FE simulations, further improving the efficiency and accuracy of surrogate model.
- Extend the proposed PCE-BI method to time-varying models, such as concrete creep and steel corrosion.
- Address such complexities by integrating non-Gaussian noise models to better capture the irregularities of actual measurement errors, enhancing the method's robustness in practical engineering applications.

## CRediT authorship contribution statement

**Zhifan Han:** Writing – original draft, Visualization, Software, Methodology, Funding acquisition, Formal analysis. **Yifei Li:** Writing – review & editing, Validation, Methodology, Funding acquisition. **Magd Abdel Wahab:** Writing – review & editing, Validation, Supervision.

## Declaration of Competing Interest

The authors declare that they have no known competing financial interests or personal relationships that could have appeared to influence the work reported in this paper.

## Acknowledgements

The authors gratefully acknowledge research funding from Guangdong Province Characteristic Innovation Projects for General Higher Education Institutions (No. 2022KTSCX169); Guangzhou Institute of Technology Key Research Projects (No. 2024KZ003); Zhejiang Key Laboratory of Industrial Solid Waste Thermal Hydrolysis Technology and Intelligent Equipment; Guangzhou Institute of Technology Research Startup Project (2025KYQ010).

## Data availability

The data that has been used is confidential.

## References

[1] Ingólfsson ET, Georgakis CT, Jönsson J. Pedestrian-induced lateral vibrations of footbridges: a literature review. Eng Struct 2012;45:21–52. https://doi.org/10.1016/j.engstruct.2012.05.038.
[2] Belykh I, Bocian M, Champneys AR, Daley K, Jeter R, Macdonald JHG, et al. Emergence of the London millennium bridge instability without synchronisation. Nat Commun 2021;12:7223. https://doi.org/10.1038/s41467-021-27568-y.
[3] Thai HT. Machine learning for structural engineering: a state-of-the-art review. Structures 2022;38:448–91. https://doi.org/10.1016/j.istruc.2022.02.003.
[4] Yu S, Huang S, Li Y, et al. Insights into the frost cracking mechanisms of concrete by using the coupled thermo-hydro-mechanical-damage meshless method[J]. Theor Appl Fract Mech 2025;136:104814. https://doi.org/10.1016/j.tafmec.2024.104814.
[5] Ding Z, Kuok SC, Lei Y, et al. Clustering driven incremental learning surrogate model-assisted evolution for structural condition assessment[J]. Mech Syst Signal Process 2025;224:112146. https://doi.org/10.1016/j.ymssp.2024.112146.
[6] Živanović S, Pavic A, Reynolds P. Finite element modelling and updating of a lively footbridge: the complete process. J Sound Vib 2007;301:126–45. https://doi.org/10.1016/j.jsv.2006.09.024.
[7] Bursi OS, Kumar A, Abbiati G, Ceravolo R. Identification, model updating, and validation of a steel twin deck curved Cable-Stayed footbridge. ComputAided Civ Infrastruct Eng 2014;29:703–22. https://doi.org/10.1111/mice.12076.
[8] Jahjouh M, Erhan S. Optimization of prestressed concrete bridge girder section using a modified harmony search algorithm. Structures 2022;46:625–36. https://doi.org/10.1016/j.istruc.2022.10.093.
[9] Wang L, Cheng L, Liu Y. Uncertainty-oriented physics-informed long short-term memory (UOPI-LSTM) network framework for dynamic force identification with interval uncertainties. Expert Syst Appl 2025;274:127067. https://doi.org/10.1016/j.eswa.2025.127067.
[10] Liu Y, Wang L, Ng BF. Multitask-Transfer-Learning method for Random-Force frequency identification considering multisource uncertainties. AIAA J 2025;63:2345–60. https://doi.org/10.2514/1.J064860.
[11] Liu Y, Wang L. Multiobjective-clustering-based optimal heterogeneous sensor placement method for thermo-mechanical load identification. Int J Mech Sci 2023;253:108369. https://doi.org/10.1016/j.ijmecsci.2023.108369.
[12] Zhang H, Wang L, Liu Y. A hybrid model-based and data-driven method for mechanical-thermal dynamic load identification considering multi-source uncertainties. Comput Methods Appl Mech Eng 2025;435:117662. https://doi.org/10.1016/j.cma.2024.117662.
[13] Liu Y, Wang L, Ng BF. Load-independent multi-objective sensor placement method for localization and reconstruction of external excitations under interval uncertainties[J]. Comput Methods Appl Mech Eng 2023;416:116344. https://doi.org/10.1016/j.cma.2023.116344.
[14] Guo X-Y, Fang S-E. Structural parameter identification using physics-informed neural networks. Measurement 2023;220:113334. https://doi.org/10.1016/j.measurement.2023.113334.
[15] Teloli RDO, Tittarelli R, Bigot M, Coelho L, Ramasso E, Moal PL, et al. A physics-informed neural networks framework for model parameter identification of beam-like structures. Mech Syst Signal Process 2025;224:112189. https://doi.org/10.1016/j.ymssp.2024.112189.
[16] Zhang R, Warn GP, Radlińska A. Physics-Informed parallel neural networks with self-adaptive loss weighting for the identification of continuous structural systems.

Comput Methods Appl Mech Eng 2024;427:117042. https://doi.org/10.1016/j.cma.2024.117042.

[17] Zhou W, Xu YF. Damage identification for plate structures using physics-informed neural networks. Mech Syst Signal Process 2024;209:111111. https://doi.org/10.1016/j.ymssp.2024.111111.

[18] Emad W, Mohammed AS, Kurda R, et al. Prediction of concrete materials compressive strength using surrogate models. Structures 2022;46:1243–67. https://doi.org/10.1016/j.istruc.2022.11.002.

[19] Kaveh A, Khavaninzadeh N. Efficient training of two ANNs using four meta-heuristic algorithms for predicting the FRP strength. Structures 2023;52:256–72. https://doi.org/10.1016/j.istruc.2023.03.17.

[20] Li C, Amanov A, Li Y, Wang C, Wang D, Abdel Wahab M. Prediction of residual stress distribution induced by ultrasonic nanocrystalline surface modification using machine learning. Adv Eng Softw 2024;188:103570. https://doi.org/10.1016/j.advengsoft.2023.103570.

[21] Roy A, Chakraborty S. Support vector regression based metamodel by sequential adaptive sampling for reliability analysis of structures. Reliab Eng Syst Saf 2020;200:106948. https://doi.org/10.1016/j.ress.2020.106948.

[22] Li Y.F., Minh H.L., Cao M.S., et al. An integrated surrogate model-driven and improved termite life cycle optimizer for damage identification in dams[J]. Mech Syst Signal Process. https://doi.org/〈10.1016/j.ymssp.2023.110986〉.

[23] Wang J, Deng J, Ren S, et al. Acoustic wave propagation characteristics and spontaneous combustion warning of coal during oxidative warming of loose coal [J]. Fuel 2025;398:135528. https://doi.org/10.1016/j.fuel.2025.135528.

[24] Li Y, Hariri-Ardebili MA, Deng T, Wei Q, Cao M. A surrogate-assisted stochastic optimization inversion algorithm: parameter identification of dams. Adv Eng Inf 2023;55:101853. https://doi.org/10.1016/j.aei.2022.101853.

[25] Shen D, Wu H, Xia B, Gan D. Polynomial chaos expansion for parametric problems in engineering systems: a review. IEEE Syst J 2020;14:4500–14. https://doi.org/10.1109/JSYST.2019.2957664.

[26] Wang Z, Ghanem R. An extended polynomial chaos expansion for PDF characterization and variation with aleatory and epistemic uncertainties. Comput Methods Appl Mech Eng 2021;382:113854. https://doi.org/10.1016/j.cma.2021.113854.

[27] Wu SQ, Law SS. Dynamic analysis of bridge with non-Gaussian uncertainties under a moving vehicle. Probabilistic Eng Mech 2011;26:281–93. https://doi.org/10.1016/j.probengmech.2010.08.004.

[28] Spiridonakos MD, Chatzi EN, Sudret B. Polynomial chaos expansion models for the monitoring of structures under operational variability. ASCEASME J Risk Uncertain Eng Syst Part Civ Eng 2016;2:B4016003. https://doi.org/10.1061/AJRUA6.0000872.

[29] Ni P, Xia Y, Li J, Hao H. Using polynomial chaos expansion for uncertainty and sensitivity analysis of bridge structures. Mech Syst Signal Process 2019;119:293–311. https://doi.org/10.1016/j.ymssp.2018.09.029.

[30] Rizzo F, Caracoglia L. Artificial neural network model to predict the flutter velocity of suspension bridges. Comput Struct 2020;233:106236. https://doi.org/10.1016/j.compstruc.2020.106236.

[31] Wan H-P, Ren W-X, Todd MD. Arbitrary polynomial chaos expansion method for uncertainty quantification and global sensitivity analysis in structural dynamics. Mech Syst Signal Process 2020;142:106732. https://doi.org/10.1016/j.ymssp.2020.106732.

[32] Shang Y, Nogal M, Teixeira R, Wolfert AR (Rogier) M. Extreme-oriented sensitivity analysis using sparse polynomial chaos expansion. Application to train–track–bridge systems. Reliab Eng Syst Saf 2024;243:109818. https://doi.org/10.1016/j.ress.2023.109818.

[33] Hu X, Fang G, Ge Y. Uncertainty propagation of flutter derivatives and structural damping in buffeting fragility analysis of long-span bridges using surrogate models. Struct Saf 2024;106:102410. https://doi.org/10.1016/j.strusafe.2023.102410.

[34] Wei X, Wan H-P, Russell J, Živanović S, He X. Influence of mechanical uncertainties on dynamic responses of a full-scale all-FRP footbridge. Compos Struct 2019;223:110964. https://doi.org/10.1016/j.compstruct.2019.110964.

[35] Pepi C, Gioffrè M, Grigoriu M. Bayesian inference for parameters estimation using experimental data. Probabilistic Eng Mech 2020;60:103025. https://doi.org/10.1016/j.probengmech.2020.103025.

[36] Zheng Y, Han F. Markov chain Monte Carlo (MCMC) uncertainty analysis for watershed water quality modeling and management. Stoch Environ Res Risk Assess 2016;30:293–308. https://doi.org/10.1007/s00477-015-1091-8.

[37] Parameter identification for damaged condition investigation on masonry arch bridges using a Bayesian approach. Eng Struct 2018;172:275–284. https://doi.org/10.1016/j.engstruct.2018.06.040..

[38] Jesus A, Brommer P, Westgate R, Koo K, Brownjohn J, Laory I. Bayesian structural identification of a long suspension bridge considering temperature and traffic load effects. Struct Health Monit 2019;18:1310–23. https://doi.org/10.1177/1475921718794299.

[39] Argyris C, Papadimitriou C, Panetsos P, Tsopelas P. Bayesian Model-Updating using features of modal data: application to the metsovo bridge. J Sens Actuator Netw 2020;9:27. https://doi.org/10.3390/jsan9020027.

[40] Ni P, Li J, Hao H, Han Q, Du X. Probabilistic model updating via variational Bayesian inference and adaptive Gaussian process modeling. Comput Methods Appl Mech Eng 2021;383:113915. https://doi.org/10.1016/j.cma.2021.113915.

[41] Liu P, Chu X, Cui W, Zhao L, Ge Y. Bayesian inference based parametric identification of vortex-excited force using on-site measured vibration data on a long-span bridge. Eng Struct 2022;266:114597. https://doi.org/10.1016/j.engstruct.2022.114597.

[42] Coelho Lima I, Robens-Radermacher A, Titscher T, Kadoke D, Koutsourelakis P-S, Unger JF. Bayesian inference for random field parameters with a goal-oriented quality control of the PGD forward model's accuracy. Comput Mech 2022;70:1189–210. https://doi.org/10.1007/s00466-022-02214-6.

[43] Crestaux T, Le Maître O, Martinez J-M. Polynomial chaos expansion for sensitivity analysis. Reliab Eng Syst Saf 2009;94:1161–72. https://doi.org/10.1016/j.ress.2008.10.008.

[44] YiFei L, MaoSen C, Tran-Ngoc H, Khatir S, Abdel Wahab M. Multi-parameter identification of concrete dam using polynomial chaos expansion and slime mould algorithm. Comput Struct 2023;281:107018. https://doi.org/10.1016/j.compstruc.2023.107018.

[45] Soize C, Ghanem R. Physical systems with random uncertainties: chaos representations with arbitrary probability measure. SIAM J Sci Comput 2004;26:395–410. https://doi.org/10.1137/S1064827503424505.

[46] Blatman G, Sudret B. Adaptive sparse polynomial chaos expansion based on least angle regression. J Comput Phys 2011;230:2345–67. https://doi.org/10.1016/j.jcp.2010.12.021.

[47] Baptista R, Stolbunov V, Nair PB. Some greedy algorithms for sparse polynomial chaos expansions. J Comput Phys 2019;387:303–25. https://doi.org/10.1016/j.jcp.2019.01.035.

[48] Borgonovo E. A new uncertainty importance measure. Reliab Eng Syst Saf 2007;92:771–84. https://doi.org/10.1016/j.ress.2006.04.015.

[49] Sandhu R, Poirel D, Pettit C, Khalil M, Sarkar A. Bayesian inference of nonlinear unsteady aerodynamics from aeroelastic limit cycle oscillations. J Comput Phys 2016;316:534–57. https://doi.org/10.1016/j.jcp.2016.03.006.

[50] Rappel H, Beex LAA, Hale JS, Noels L, Bordas SPA. A tutorial on Bayesian inference to identify material parameters in solid mechanics. Arch Comput Methods Eng 2020;27:361–85. https://doi.org/10.1007/s11831-018-09311-x.

[51] Babuška I, Sawlan Z, Scavino M, Szabó B, Tempone R. Bayesian inference and model comparison for metallic fatigue data. Comput Methods Appl Mech Eng 2016;304:171–96. https://doi.org/10.1016/j.cma.2016.02.013.

[52] Ding Y-J, Wang Z-C, Chen G, Ren W-X, Xin Y. Markov chain monte Carlo-based Bayesian method for nonlinear stochastic model updating. J Sound Vib 2022;520:116595. https://doi.org/10.1016/j.jsv.2021.116595.

[53] Wang L, Shi W, Zhang Q, Zhou Y. Study on adaptive-passive multiple tuned mass damper with variable mass for a large-span floor structure. Eng Struct 2020;209:110010. https://doi.org/10.1016/j.engstruct.2019.110010.

[54] Li Z, Li D, Lu Y, Cheng K, Wu Q. Serviceability analysis of a cable-supported footbridge subjected to human-induced loads. Int J Struct Integr 2019;11:497–513. https://doi.org/10.1108/IJSI-09-2019-0092.

[55] Bedon C. Experimental investigation on vibration sensitivity of an indoor glass footbridge to walking conditions. J Build Eng 2020;29:101195. https://doi.org/10.1016/j.jobe.2020.101195.

[56] Bedon C. Diagnostic analysis and dynamic identification of a glass suspension footbridge via on-site vibration experiments and FE numerical modelling. Compos Struct 2019;216:366–78. https://doi.org/10.1016/j.compstruct.2019.03.005.

[57] Hariri-Ardebili MA, Sudret B. Polynomial chaos expansion for uncertainty quantification of dam engineering problems[J]. Eng Struct 2020;203:109631. https://doi.org/10.1016/j.engstruct.2019.109631.

[58] Minh H-L, Khatir S, Abdel Wahab M, Cuong-Le T. An enhancing particle swarm optimization algorithm (EHVPSO) for damage identification in 3D transmission tower. Eng Struct 2021;242:112412. https://doi.org/10.1016/j.engstruct.2021.112412.

[59] Zhang Z, He X, AlSinan M, Kwak H, Hoteit H. Robust method for reservoir simulation history matching using Bayesian inversion and Long-Short-Term memory Network-Based proxy. SPE J 2023;28:983–1007. https://doi.org/10.2118/203976-PA.